Swimming *Escherichia coli* Cells Explore the Environment by Lévy Walk

Haiyan Huo,[a,b] Rui He,[a] Rongjing Zhang,[a] (ID) Junhua Yuan[a]

[a]Hefei National Laboratory for Physical Sciences at the Microscale and Department of Physics, University of Science and Technology of China, Hefei, Anhui, China
[b]Department of Basic Education, Hohhot Institute of Nationalities, Hohhot, China

ABSTRACT *Escherichia coli* cells swim in aqueous environment in a random walk of alternating runs and tumbles. The diffusion characteristics of this random walk remains unclear. In this study, by tracking the swimming of wild-type cells in a three-dimensional (3D) homogeneous environment, we found that their trajectories are superdiffusive, consistent with Lévy walk behavior. For comparison, we tracked the swimming of mutant cells that lack the chemotaxis signaling noise (the steady-state fluctuation of the concentration of the chemotaxis response regulator CheY-P) and found that their trajectories are normal diffusive. Therefore, wild-type *E. coli* cells explore the environment by Lévy walk, which originates from the chemotaxis signaling noise. This Lévy walk pattern enhances their efficiency in environmental exploration.

IMPORTANCE *E. coli* cells explore the environment in a random walk of alternating runs and tumbles. By tracking the 3D trajectories of *E. coli* cells in an aqueous environment, we found that their trajectories are superdiffusive, with a power-law shape for the distribution of run lengths, which is characteristics of Lévy walk. We further show that this Lévy walk behavior is due to the random fluctuation of the output level of the bacterial chemotaxis pathway, and it enhances the efficiency of the bacteria in exploring the environment.

KEYWORDS chemotaxis, diffusion, flagellar motor, run and tumble

Bacteria with peritrichous flagella, such as *Escherichia coli*, can swim in aqueous environments in a pattern of three-dimensional (3D) random walk, which can be summarized as a repetitive process of a smooth movement interrupted by a sudden turn (1). The smooth movement, also called a run, occurs when all flagella rotate in counterclockwise (CCW) direction and thus form a helical bundle. The sudden turn, also regarded as a tumble, occurs when one or more of the flagella rotate in clockwise (CW) direction, which leads to disassembly of the bundle (2, 3). The rotation direction is modulated by phosphorylated CheY (CheY-P) (4), the concentration of which is regulated by the chemotaxis transduction network (5, 6). Through the chemotaxis network, bacteria can move toward nutrient sources and avoid repellents. In the network, external stimuli are sensed by transmembrane chemoreceptor clusters that locate at cell poles, which modulate the activity of the associated kinase CheA. When in the active state, CheA can transfer the phosphor group to CheY, whereas the CheZ phosphatase binds to CheY-P and accelerates its dephosphorylation. CheY-P diffuses and binds to the switch complex at the base of the flagellar motor, increasing the probability that the motor spins CW (4, 7, 8). The methyltransferase CheR and methylesterase CheB implement the adaptation process by tuning the methylation level to modulate the activity of receptors, forming a negative-feedback loop (9). Due to stochastic fluctuation of the adaptation process and the receptor-kinase dynamics, the output of the chemotaxis network, i.e., CheY-P concentration, exhibits strong temporal fluctuations (10–12). The relative magnitude and the relaxation timescale

of the fluctuation the motors sense are about 10% and 10 s, respectively, as estimated from a recent experiment (13).

Lévy walk is a mode of random movement, in which the walkers move a distance l along a direction at a constant velocity and then choose a new direction randomly for the next move. The distribution of the distance l per straight segment follows power-law distribution with a heavy tail: $P(l) = al^{-\mu}$, where μ ($1 < \mu \leq 3$) is the power-law exponent. With this mode of random walk, the trace of the walker exhibits a fractal pattern (14). Many species perform Lévy walks when searching for food or preying (15–18). It is an efficient strategy for searching for randomly and sparsely distributed food, benefitting from its properties of fractal and superdiffusiveness (14).

In the canonical run-and-tumble behavior of *E. coli* swimming, the bacteria were found to be essentially following a normal diffusive motion (1, 19), and the distribution of run length (or run duration, as the run speed is constant) was exponential (1). Previous single-motor observation of motor switching kinetics in *E. coli* showed that distribution of the motor CCW duration exhibited a power-law tail (20), which stemmed from fluctuation of CheY-P concentration that originated from the stochastic activities of CheR and CheB as explained by several theoretical and simulation studies (12, 21–23). However, there is no strict one-to-one correspondence between motor CCW rotation and cell running due to the complex dynamics of flagellar bundle formation and dispersal, and changing to CW rotation by any one of the multiple motors on a cell induces a tumble and disrupts a possible long run (24). It therefore remains to be seen directly whether the distribution of run length exhibits a power-law shape. A previous study showed that swarming (on a wet agar surface) *Bacillus subtilis* and *Serratia marcescens* exhibited Lévy walk behavior, characterized by the power-law shape of the distribution of duration between sharp turns in the cell trajectories (18). However, a recent study found that swarming *E. coli* exhibited normal diffusive behavior showing an exponential shape of the distribution of duration between sharp turns (25). Therefore, it is intriguing what the behavior is for *E. coli* swimming in a 3-dimensional liquid environment.

In this work, we carried out 3D tracking experiments for *E. coli* swimming in a homogeneous environment (without gradients of chemo stimuli). We compared the swimming behaviors of two strains, a strain that is wild type for chemotaxis and a mutant strain that lacks the fluctuation of CheY-P concentration (as its CheY proteins were replaced with a double mutant that was active without phosphorylation, and the level of the mutant protein was stable over the experiments). Our results show that the trajectories of the wild-type *E. coli* are superdiffusive, consistent with Lévy walk behavior, whereas those of the mutant *E. coli* are normal diffusive. This suggest that the fluctuation of the CheY-P concentration is the origin of the Lévy walk behavior. We further demonstrate that the Lévy walk pattern of swimming *E. coli* allows the bacteria to explore the environment more effectively.

RESULTS

We sought to compare the swimming behavior of the wild-type strain RP437 and the mutant HCB900, which lacks the fluctuation of CheY-P concentration. HCB900 is a derivative of RP437, with a defective chemotaxis network and with the *cheY* gene replaced with a mutant allele that expresses CheY[13DK106YW] (a CheY double mutant that is active without phosphorylation) under the control of the isopropyl-β-D-thiogalactoside (IPTG)-inducible promoter (26). To ensure similar average CW biases (the probability of motor turning CW) for the wild-type and the mutant cells, we performed a bead assay to measure the CW bias distributions of both strains. We used JY26 as the wild-type strain, which was generated by deleting the filament gene *fliC* from RP437 and transforming it with a plasmid that expresses the sticky filament FliC[st]. We used HCB901 as the mutant strain, which was generated similarly from HCB900. By adjusting the concentration of the inducer, we were able to obtain similar distributions of CW biases for both strains (see Fig.
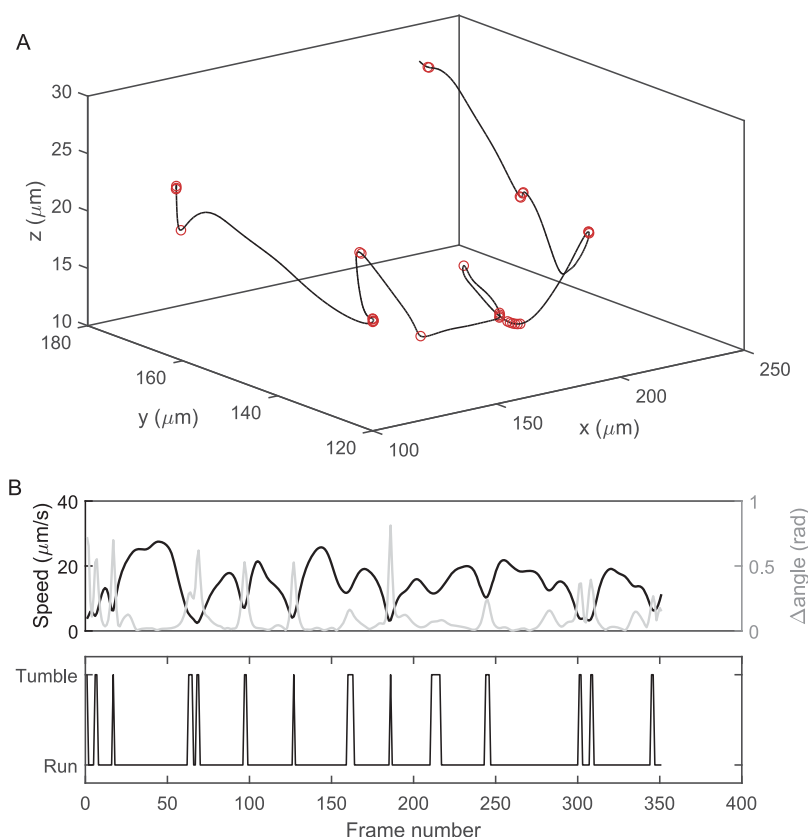
FIG 1 An example of swimming trajectory with detected run and tumble events, recorded for 14.04 s at 25 frames per second. (A) The 3D trajectory of the bacterium, with the tumble events indicated by open circles. (B) The instantaneous speed (black line) and angular change (gray line) at each frame (top panel) and the detected run and tumble states for each frame (bottom panel).

S1 in the supplemental material). This inducer concentration (24 μM IPTG) was used in subsequent experiments.

To track bacterial swimming in 3D, we exploited the defocused particle tracking technique (19, 27), but with bacterial images (bright rings) produced by dark-field microscopy rather than fluorescence. By calibrating the relationship between the z position and the ring sizes, we can get the z positions for individual bacteria by measuring the ring sizes, and we can get the x and y positions from the center of the rings. We recorded videos of bacterial swimming using dark-field microscopy. The videos were analyzed by using custom MATLAB scripts (https://github.com/NameMor/Bacteria-3D -track) to extract the trajectories for individual bacteria. Trajectories longer than 10 s were used for further analysis. A total of 1,668 trajectories with a total time of 477.512 min were obtained for HCB900 cells, and 1,264 trajectories with a total time of 314.824 min were obtained for RP437 cells. We used both the swimming speed and the velocity angular change between adjacent frames (proportional to angular speed) as criteria to identify tumbles in a trajectory (see Materials and Methods for further details). An example of swimming trajectory with identified run and tumble events is shown in Fig. 1. The average run speed for either strain was about 10 μm/s.

The mean square displacement (MSD) of a random walker characterizes its diffusive property. The relationship of MSD versus lag time *t* (the duration of time for which the displacement is calculated) can be described by the power-law form: MSD = $D \times t^{\alpha}$, where α of values $0 < \alpha < 1$, 1, and $\alpha > 1$ indicate subdiffusion, normal diffusion, and superdiffusion, respectively. We calculated the ensemble-averaged MSD for the trajectories of RP437 and HCB900, as shown in Fig. 2. The MSDs for all of the trajectories are
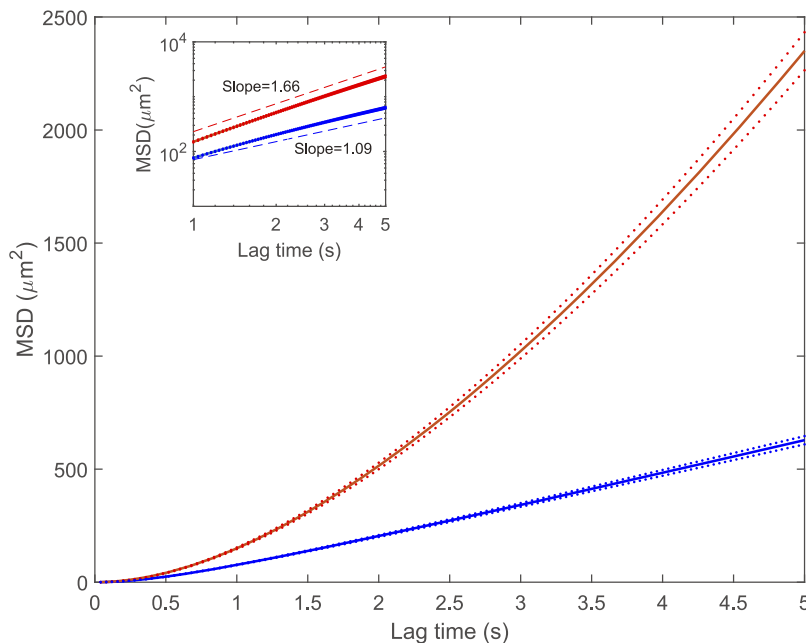
FIG 2 The ensemble-averaged MSD as a function of lag time for both strains. Red lines, the wild-type RP437 (average of 1,264 trajectories with a total time of 314.824 min); blue lines, the mutant HCB900 (average of 1,668 trajectories with a total time of 477.512 min). The dotted lines show the regions of SEM. The inset shows the corresponding log-log plot, with the dashed lines indicating the slopes.

shown in Fig. S2. We used the power-law form to fit the curve of RP437, and the power-law exponent α was extracted to be 1.66 ± 0.01, whereas it was ~1 for HCB900 (1.09 ± 0.01). Therefore, the trajectories of RP437 are superdiffusive, whereas those of HCB900 are normal diffusive.

Wild-type cells exhibit large cell-to-cell variability in terms of statistics of CW and CCW duration (20). To characterize some of the cell-to-cell variability for RP437 cells in terms of their swimming pattern, we calculated the average run time for each trajectory and plotted the distribution of average run time (Fig. S3, inset). To see the effect of this variability on the exploratory behavior, we sorted the trajectories into three groups according to the average run time: <1.18 s, between 1.18 and 1.25 s, and >1.25 s; we then calculated the ensemble-averaged MSD as a function of lag time for each group. The superdiffusive behaviors for the groups are similar (Fig. S3), with similar fitted values of α of 1.67 ± 0.01, 1.64 ± 0.01, and 1.68 ± 0.01 for the groups with average run times of <1.18 s, between 1.18 and 1.25 s, and >1.25 s, respectively.

To investigate further properties of the swimming behavior, we extracted the run durations from the trajectories and plotted the distributions of run durations for RP437 and HCB900 (Fig. 3). From the semi-log plot of the distributions shown in the inset of Fig. 3A, the tail of the distribution for the mutant HCB900 is nearly a straight line, clearly exhibiting an exponential shape. This is consistent with the normal diffusive behavior of HCB900 cells. In the log-log plot in Fig. 3, the tail of the distribution for the wild-type RP437 cells is a straight line, decaying in a power-law fashion $t^{-\mu}$ with μ having a value of 2.29 ± 0.16. This agrees excellently with the theory of Lévy walk, which predicts that $\alpha + \mu = 4$ (28).

As a further test of the Lévy walk pattern for the trajectories of RP437 cells, we calculated the distribution of cell displacements during a fixed time interval, Δt. The theory of Lévy walk predicts that the distributions of displacements for different Δt's fall on the same curve if the displacements are scaled by Δt^γ, where $\gamma = 1/(3 - \alpha)$. This is clearly demonstrated in our experimental data for RP437, as shown in Fig. 3B.

From the normal diffusive behavior for the trajectories of the mutant HCB900 cells,
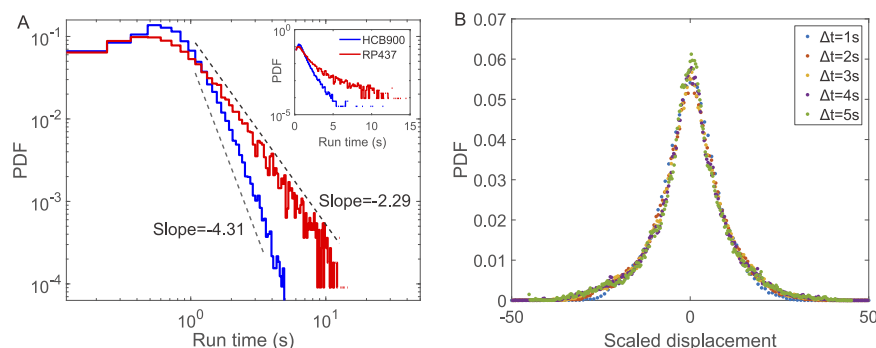
FIG 3 The trajectories of RP437 are consistent with Lévy walks. (A) The distributions of run times for the two strains (red line, RP437; blue line, HCB900). The inset shows the semi-log plot. PDF, probability density function. (B) The distribution of the displacements during fixed time interval Δt, scaled by Δt^{γ}.

and the Lévy walk behavior for those of the wild-type RP437 cells, the stochastic fluctuation of CheY-P concentration (signaling noise) inherent in the wild-type cells seems to be the reason for this Lévy walk behavior. To see it more clearly, we performed a stochastic simulation of bacterial swimming in the presence or absence of the signaling noise. The fluctuation of the CheY-P concentration at a steady state was described using the Langevin equation with the parameters τ and σ, the relaxation time and the magnitude of the fluctuation, respectively (13, 21). With the values of τ of 10 s, σ of 0.26 μM, and motor sensitivity of 20 for the Hill coefficient as determined previously (13, 29, 30), we reproduced the behavior of cells with (RP437) and without (HCB900) noise. As shown in Fig. S4A, the tail of the run-time distribution of cells with noise is a power-law shape with a μ value of 2.3, whereas that of cells without noise is an exponential shape. The MSD as a function of the lag time demonstrates that the trajectories for cells with noise are superdiffusive (with α of 1.62), whereas those for cells without noise are normal diffusive (Fig. S4B).

DISCUSSION

In this study, we showed that the swimming behavior of wild-type cells with chemotaxis signaling noise (fluctuation of CheY-P concentration) is superdiffusive, consistent with a Lévy walk pattern, whereas that of mutant cells without noise is normal diffusive. By combining experimental 3D tracking of cell swimming with stochastic simulations, we revealed that the signaling noise induces the Lévy walk behavior of the wild-type cells.

The chemotaxis signaling noise was shown to have originated from stochastic activities of the adaptation enzymes (12) and interactions among the clustered receptors that may generate giant fluctuations of kinase activity (10, 11) and induce transient CheY-P pulses (31, 32). Although the nature of the signaling noises at the receptor patches was not well characterized, the fluctuation of CheY-P level that the flagellar motors sense ultimately comes from the noise at the receptor patches that diffuses to where the motors are located. The fact that our simulation reproduced the exploratory pattern for the wild-type cells and the mutant cells without noise suggested that most of properties of the CheY-P fluctuation the motors sense could be described by the Langevin equation.

It was demonstrated previously that the chemotaxis signaling noise helps to coordinate the rotation of multiple flagellar motors that grow on a bacterium (33, 34) and enhances the chemotactic drift in chemical gradients and the sensitivity of the chemotaxis network (13, 34, 35). In this investigation we showed that the signaling noise can also promote superdiffusion for cells in a homogeneous environment, resulting in Lévy walk behavior.
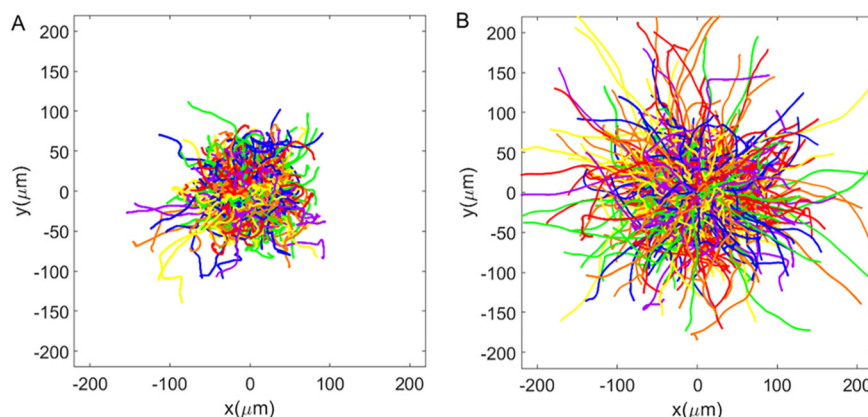
FIG 4 The spreading of mutant HCB900 (A) and the wild-type RP437 (B) cells within 10 s. Each line indicates a 10-s trajectory with the start repositioned to the origin.

Lévy walk is an efficient strategy for searching for randomly and sparsely distributed food. The Lévy walk pattern of *E. coli* swimming helps its exploration of the environment. To show that, we plotted the first 10-s section of all the trajectories together, repositioning the start of the trajectories to the origin. As shown in Fig. 4 for the trajectories of the mutant and the wild-type cells, the wild-type cells were able to explore a much wider region within the same period. This demonstrated that the Levy walk behavior of wild-type cells is a more efficient exploration strategy than the normal diffusive behavior of the mutant cells.

In summary, *E. coli* cells explore the environment efficiently by Lévy walk. We expect to see similar motility behavior in other microorganisms.

MATERIALS AND METHODS

Strains and plasmids. *E. coli* strain RP437 is wild type for chemotaxis. Strains HCB900 (Δ*cheA cheZ cat* Ptrc$_{420}$ *che*Y^{13DK106YW}), HCB901 (Δ*cheA cheZ fliC cat* Ptrc$_{420}$*che*Y^{13DK106YW}) (26), and JY26 (Δ*fliC*) are derivatives of RP437. The plasmid pBES38 constitutively expresses both LacI^q and the sticky filament FliCst (26). The plasmid pTrc99a expresses LacI^q. The plasmid pKAF131 constitutively expresses sticky filament FliCst. HCB901 transformed with pBES38 and JY26 transformed with pKAF131 were used for the bead assay. HCB900 transformed with pTrc99a and RP437 were used for the 3D tracking experiments.

Experiment procedure. Cells were grown at 33°C in T-broth with the appropriate antibiotics (170 μg/ml of chloramphenicol and 100 μg/ml of ampicillin). For HCB900 and HCB901 cultures, 24 μM IPTG was added to the culture solution when grown to an optical density at 600 nm (OD$_{600}$) of 0.38 ± 0.02. When the cells were grown to an OD$_{600}$ between 0.45 and 0.50, 1 ml of HCB901 or JY26 culture solution was centrifuged at 4,000 × g for 1 min twice with motility medium to collect the cells and resuspended in a final volume of 1 ml. To reduce the breakage of flagella, the centrifugation was performed once at 1,200 × g for 5 min when harvesting HCB900 and HCB33 cells, and gentle pipetting was used to resuspend the cells after centrifugation.

Bead assay. To perform the bead assays, cells were handled as described previously (13). Briefly, cells were sheared to truncate flagella by passing 1 ml of the washed-cell suspension 80 times between two syringes equipped with 23-gauge needles and connected by a 7-cm-long section of polyethylene tubing (0.58-mm inside diameter [i.d.], no. 427411; Becton, Dickinson, Franklin Lakes, NJ). Polystyrene latex beads (1.0-mm-diameter, no. 07310; Polysciences, Warrington, PA) were then attached to the sticky flagellar stubs by passive adsorption. The polystyrene beads were observed by phase-contrast microscopy equipped with a ×40 objective, and the motion of beads was recorded with a complementary metal oxide semiconductor (CMOS) camera (DCC3240M; Thorlabs) for two and half minutes at a frame rate of 500 Hz with a reduced region of interest that covered the trajectory of the beads.

3D tracking. To perform the tracking experiment, we used the defocused particle tracking technique as described previously (19); the technique exploits the emerged ring of particles when they deviate from the focal plane. In this study, the imaging was performed with dark-field microscopy. To let cells swim freely in three dimensions, a sample chamber was constructed with two pieces of coverslips using 1-mm-thick double-sided tape as spacer. Then the swimming videos were recorded with the same camera as in the bead assay at a frame rate of 25 Hz, an exposure time of 35 ms, and a gain of ×33. The focal plane was set near the middle plane between the two coverslips. Dark-field microscopy was achieved by using a Nikon Ti-E phase-contrast microscope equipped with a ×20 objective (numerical aperture [NA], 0.45), a high-NA condenser (NA, 0.72), and a ph4 phase ring. The size of the field of view was 339.20 by 271.36 μm^2. All of the experiments were done at 23°C.

Data processing. Data analysis was performed with custom scripts in MATLAB. For the data from the bead assay, the position of the bead in each frame of a video was calculated as the averaged pixel position weighted by the intensity of the pixels. Then angular positions were calculated by connecting the bead positions to the center of the bead trajectory, and subsequently, the angular velocities were calculated. The velocity time traces were converted to binary time traces of CW and CCW states, using the threshold-crossing algorithm described previously (36). For each motor trace, the CW bias was calculated as the mean CW interval divided by the sum of the mean CW and CCW intervals.

For the data from the tracking experiments, each frame of the video was analyzed to get the *xy* positions and the radius of the image circle that resulted from cell defocusing. Then, using the calibrated linear relationship between the radius and the *z* defocusing distance, we could get the *z* positions of the cells. A cell trajectory was connected by comparing the distances between the position of the cell in present frame and the positions of all cells in the next frame. The cell trajectories were smoothed with the à trous wavelet filter (37). From the trajectories of individual cells, we calculated the swimming velocities at each frame and the velocity angular changes between adjacent frames (proportional to angular speeds). To detect tumble events in the trajectories, an algorithm described previously was used (38–40). The basic idea is to use the decrease of swimming speeds and increase of angular speeds to determine the tumble event. The local maximum of the speed decrease is characterized as $\Delta v = \max [v(t_1) - \nu(t_{min}), \nu(t_2) - \nu(t_{min})]$, where t_{min} is the time at which a local minimum of swimming speed is located and $\nu(t_1)$ and $\nu(t_2)$ are the closest local maxima located around t_{min}. The local maximum of the increase of angular speed is characterized as $\Delta\omega = [\omega(t_{max\_a}) - \omega(t_{1a}), \omega(t_{max\_a}) - \omega(t_{2a})]$, where $\omega(t_{1a})$ is the local maximum of the angular speed and $\omega(t_{1a})$ and $\omega(t_{2a})$ are the closest local minima. If $\Delta v/v(t_{min}) > 0.5$, and the angular change between t_{1a} and t_{2a} exceeds $2[4D_{rot}(t_{2a} - t_{1a})]^{1/2}$, where $D_{rot} = 0.1$ rad^2/s is the rotation diffusion coefficient of the cell body, then a tumble event occurs around t_{min}, and the tumble duration is set to the period during which $v(t) - v(t_{min}) \leq 0.2\Delta v$ and $\omega(t_{max\_a}) - \omega(t) \leq 0.2\Delta\omega$.

Simulations. Each cell transits stochastically between run and tumble; the transition rate from run to tumble is $B/0.11$, same as the switching rate of the flagellar motor from CCW to CW (13), where B is the motor CW bias, calculated from the Hill equation $B = Y^N/(Y^N + 3.1^N)$ with a Hill coefficient N of 20 (30). The transition rate from tumble to run is set to be 5 s^{-1}. The fluctuation of CheY-P concentration was updated using the Ornstein-Uhlenbeck formula (13, 41, 42):

$$\Delta Y(t+dt) = \Delta Y(t) \times e^{-dt/\tau} + \sigma \times \sqrt{1-e^{-2dt/\tau}} \times n(0,1)$$

where $n(0,1)$ is a Gaussian random number with a zero mean value and unit variance, τ is the relaxation time (measured to be ~10 s), and σ is the magnitude of fluctuation (measured to be ~0.26 μM when the CW bias is around 0.15) (29). The simulation is updated every 0.01 s, the position is recorded at the frame rate of 25 Hz, and the running speed of bacteria is set to unit speed. Each cell was simulated for 200 s, and 2,000 cells were simulated for each type of cells.

SUPPLEMENTAL MATERIAL

Supplemental material is available online only.
SUPPLEMENTAL FILE 1, PDF file, 0.3 MB.

REFERENCES

1. Berg HC, Brown DA. 1972. Chemotaxis in Escherichia coli analysed by three-dimensional tracking. Nature 239:500–504. https://doi.org/10.1038/239500a0.

2. Turner L, Ryu WS, Berg HC. 2000. Real-time imaging of fluorescent flagellar filaments. J Bacteriol 182:2793–2801. https://doi.org/10.1128/jb.182.10.2793-2801.2000.

3. Berg HC. 2003. The rotary motor of bacterial flagella. Annu Rev Biochem 72:19–54. https://doi.org/10.1146/annurev.biochem.72.121801.161737.

4. Welch M, Oosawa K, Aizawa SI, Eisenbach M. 1993. Phosphorylation-dependent binding of a signal molecule to the flagellar switch of bacteria.

Proc Natl Acad Sci U S A 90:8787–8791. https://doi.org/10.1073/pnas.90.19.8787.

5. Wadhams GH, Armitage JP. 2004. Making sense of it all: bacterial chemotaxis. Nat Rev Mol Cell Biol 5:1024–1037. https://doi.org/10.1038/nrm1524.

6. Tu Y. 2013. Quantitative modeling of bacterial chemotaxis: signal amplification and accurate adaptation. Annu Rev Biophys 42:337–359. https://doi.org/10.1146/annurev-biophys-083012-130358.

7. Cluzel P, Surette M, Leibler S. 2000. An ultrasensitive bacterial motor revealed by monitoring signaling proteins in single cells. Science 287:1652–1655. https://doi.org/10.1126/science.287.5458.1652.

8. Sourjik V, Berg HC. 2002. Binding of the Escherichia coli response regulator

CheY to its target measured *in vivo* by fluorescence resonance energy transfer. Proc Natl Acad Sci U S A 99:12669–12674. https://doi.org/10.1073/pnas.192463199.

9. Barkai N, Leibler S. 1997. Robustness in simple biochemical networks. Nature 387:913–917. https://doi.org/10.1038/43199.

10. Colin R, Rosazza C, Vaknin A, Sourjik V. 2017. Multiple sources of slow activity fluctuations in a bacterial chemosensory network. Elife 6:e26796. https://doi.org/10.7554/eLife.26796.

11. Keegstra JM, Kamino K, Anquez F, Lazova MD, Emonet T, Shimizu TS. 2017. Phenotypic diversity and temporal variability in a bacterial signaling network revealed by single-cell FRET. Elife 6:e27455. https://doi.org/10.7554/eLife.27455.

12. Emonet T, Cluzel P. 2008. Relationship between cellular response and behavioral variability in bacterial chemotaxis. Proc Natl Acad Sci U S A 105:3304–3309. https://doi.org/10.1073/pnas.0705463105.

13. He R, Zhang RJ, Yuan JH. 2016. Noise-induced increase of sensitivity in bacterial chemotaxis. Biophys J 111:430–437. https://doi.org/10.1016/j.bpj.2016.06.013.

14. Lewis M, Maini PK, Petrovskii SV. 2013. Dispersal, individual movement and spatial ecology: a mathematical perspective. Springer, Heidelberg, Germany.

15. Harris TH, Banigan EJ, Christian DA, Konradt C, Wojno EDT, Norose K, Wilson EH, John B, Weninger W, Luster AD, Liu AJ, Hunter CA. 2012. Generalized Levy walks and the role of chemokines in migration of effector CD8(+) T cells. Nature 486:545–548. https://doi.org/10.1038/nature11098.

16. Reynolds AM, Smith AD, Menzel R, Greggers U, Reynolds DR, Riley JR. 2007. Displaced honey bees perform optimal scale-free search flights. Ecology 88:1955–1961. https://doi.org/10.1890/06-1916.1.

17. de Jager M, Weissing FJ, Herman PMJ, Nolet BA, van de Koppel J. 2011. Levy walks evolve through interaction between movement and environmental complexity. Science 332:1551–1553. https://doi.org/10.1126/science.1201187.

18. Ariel G, Rabani A, Benisty S, Partridge JD, Harshey RM, Be'er A. 2015. Swarming bacteria migrate by Levy walk. Nat Commun 6:8396. https://doi.org/10.1038/ncomms9396.

19. Wu M, Roberts JW, Kim S, Koch DL, DeLisa MP. 2006. Collective bacterial dynamics revealed using a three-dimensional population-scale defocused particle tracking technique. Appl Environ Microbiol 72:4987–4994. https://doi.org/10.1128/AEM.00158-06.

20. Korobkova E, Emonet T, Vilar JMG, Shimizu TS, Cluzel P. 2004. From molecular noise to behavioural variability in a single bacterium. Nature 428:574–578. https://doi.org/10.1038/nature02404.

21. Tu Y, Grinstein G. 2005. How white noise generates power-law switching in bacterial flagellar motors. Phys Rev Lett 94:208101. https://doi.org/10.1103/PhysRevLett.94.208101.

22. Matthaus F, Jagodic M, Dobnikar J. 2009. *E. coli* superdiffusion and chemotaxis—search strategy, precision, and motility. Biophys J 97:946–957. https://doi.org/10.1016/j.bpj.2009.04.065.

23. Matthaus F, Mommer MS, Curk T, Dobnikar J. 2011. On the origin and characteristics of noise-induced Lévy walks of *E. coli*. PLoS One 6:e18623. https://doi.org/10.1371/journal.pone.0018623.

24. Darnton NC, Turner L, Rojevsky S, Berg HC. 2007. On torque and tumbling in swimming *Escherichia coli*. J Bacteriol 189:1756–1764. https://doi.org/10.1128/JB.01501-06.

25. Wu Z, He R, Zhang R, Yuan J. 2020. Swarming motility without flagellar motor switching by reversal of swimming direction in *E. coli*. Front Microbiol 11:1042. https://doi.org/10.3389/fmicb.2020.01042.

26. Scharf BE, Fahrner KA, Turner L, Berg HC. 1998. Control of direction of flagellar rotation in bacterial chemotaxis. Proc Natl Acad Sci U S A 95:201–206. https://doi.org/10.1073/pnas.95.1.201.

27. Wu M, Roberts JW, Buckley M. 2005. Three-dimensional fluorescent particle tracking at micron-scale using a single camera. Exp Fluids 38:461–465. https://doi.org/10.1007/s00348-004-0925-9.

28. Zaburdaev V, Denisov S, Klafter J. 2015. Lévy walks. Rev Mod Phys 87:483–530. https://doi.org/10.1103/RevModPhys.87.483.

29. Park H, Pontius W, Guet CC, Marko JF, Emonet T, Cluzel P. 2010. Interdependence of behavioural variability and response to small stimuli in bacteria. Nature 468:819–823. https://doi.org/10.1038/nature09551.

30. Yuan J, Berg HC. 2013. Ultrasensitivity of an adaptive bacterial motor. J Mol Biol 425:1760–1764. https://doi.org/10.1016/j.jmb.2013.02.016.

31. Terasawa S, Fukuoka H, Inoue Y, Sagawa T, Takahashi H, Ishijima A. 2011. Coordinated reversal of flagellar motors on a single Escherichia coli cell. Biophys J 100:2193–2200. https://doi.org/10.1016/j.bpj.2011.03.030.

32. Che Y-S, Sagawa T, Inoue Y, Takahashi H, Hamamoto T, Ishijima A, Fukuoka H. 2020. Fluctuations in intracellular CheY-P concentration coordinate reversals of flagellar motors in E. coli. Biomolecules 10:1544. https://doi.org/10.3390/biom10111544.

33. Hu B, Tu Y. 2013. Coordinated switching of bacterial flagellar motors: evidence for direct motor-motor coupling? Phys Rev Lett 110:158703. https://doi.org/10.1103/PhysRevLett.110.158703.

34. Sneddon MW, Pontius W, Emonet T. 2012. Stochastic coordination of multiple actuators reduces latency and improves chemotactic response in bacteria. Proc Natl Acad Sci U S A 109:805–810. https://doi.org/10.1073/pnas.1113706109.

35. Flores M, Shimizu TS, ten Wolde PR, Tostevin F. 2012. Signaling noise enhances chemotactic drift of E. coli. Phys Rev Lett 109:148101. https://doi.org/10.1103/PhysRevLett.109.148101.

36. Yuan J, Fahrner KA, Berg HC. 2009. Switching of the bacterial flagellar motor near zero load. J Mol Biol 390:394–400. https://doi.org/10.1016/j.jmb.2009.05.039.

37. Dutilleux P. 1989. An implementation of the "algorithme a trous" to compute the wavelet transform, p 298–304. *In* Combes J-M, Grossmann A, Tchamitchian P (ed), Wavelets: time-frequency methods and phase space, 2nd ed. Springer, Berlin, Germany.

38. Masson JB, Voisinne G, Wong-Ng J, Celani A, Vergassola M. 2012. Noninvasive inference of the molecular chemotactic response using bacterial trajectories. Proc Natl Acad Sci U S A 109:1802–1807. https://doi.org/10.1073/pnas.1116772109.

39. Najafi J, Shaebani MR, John T, Altegoer F, Bange G, Wagner C. 2018. Flagellar number governs bacterial spreading and transport efficiency. Sci Adv 4:eaar6425. https://doi.org/10.1126/sciadv.aar6425.

40. Theves M, Taktikos J, Zaburdaev V, Stark H, Beta C. 2013. A bacterial swimmer with two alternating speeds of propagation. Biophys J 105:1915–1924. https://doi.org/10.1016/j.bpj.2013.08.047.

41. Park H, Oikonomou P, Guet CC, Cluzel P. 2011. Noise underlies switching behavior of the bacterial flagellum. Biophys J 101:2336–2340. https://doi.org/10.1016/j.bpj.2011.09.040.

42. Gillespie DT. 1996. The mathematics of Brownian motion and Johnson noise. Am J Phys 64:225–240. https://doi.org/10.1119/1.18210.